THESIS FOR THE DEGREE OF LICENTIATE OF ENGINEERING

Braking Distance Minimization on Roads with Varying Friction

Ektor Karyotakis

Department of Electrical Engineering
Chalmers University of Technology
Gothenburg, Sweden, 2025

Braking Distance Minimization on Roads with Varying Friction

Ektor Karyotakis

Acknowledgments, dedications, and similar personal statements in this thesis, reflect the author's own views.

Thesis of Licentiate of Engineering 2025:05

Department of Electrical Engineering
Chalmers University of Technology
SE-412 96 Gothenburg, Sweden
Phone: +46 (0)31 772 1000

Cover:
A vehicle on an icy road: Lateral movement can help avoid slipperiness. Learn more on p. 33.

Printed by Chalmers Digital Printing
Gothenburg, Sweden, May 2025

Braking Distance Minimization on Roads with Varying Friction

Ektor Karyotakis
Department of Electrical Engineering
Chalmers University of Technology

Abstract

Braking safely and efficiently becomes especially challenging when road friction is uneven—for example, when one side of the car is on ice while the other is on asphalt. This situation, known as *split friction*, can cause vehicles to veer off course unless both braking and steering are carefully controlled.

This thesis explores how optimizing both braking and steering can minimize stopping distances on split friction roads. By using mathematical optimization and vehicle simulations, the research shows that traditional braking systems, like ABS, work well when the friction difference between the left and right wheels is small. However, on more extreme split friction surfaces, a more advanced approach is needed—allowing slightly higher slip at the low-friction wheels and adjusting steering to maintain stability. A proposed control method, tested in simulations, reduces stopping distances by up to 13% compared to professional human drivers.

The research also investigates how a vehicle's path can be optimized when friction varies across the road, such as when avoiding an icy patch. Results show that even a simplified vehicle model can accurately predict optimal paths, offering a fast and efficient way to enhance automated braking and path-planning systems.

These findings could help improve the safety and performance of future driver assistance systems, ensuring vehicles can stop faster and more predictably in challenging road conditions.

Keywords: Braking distance, minimization, road friction, varying friction, vehicle dynamics, split friction, steering control, stopping distance, path optimization.

To my wife, Alexandra, and to Simone, my most loyal companion,
for being my unwavering constants throughout this journey.

List of Publications

This thesis is based on the following publications:

[A] **Ektor Karyotakis**, Derong Yang, Mats Jonasson, Jonas Sjöberg, "Experimental Study on Road Friction Variation and Stopping Distance Uncertainty using ABS Braking Data". Presented in *AVEC'22*, `https://research.chalmers.se/en/publication/534217`.

[B] **Ektor Karyotakis**, Mats Jonasson, Derong Yang, Jonas Sjöberg, "Minimum Stopping Distance on Split Friction Roads via Joint Control of Steering and Individual Wheel Braking". Submitted to *Vehicle System Dynamics*, in Sept. 2024.

[C] **Ektor Karyotakis**, Derong Yang, Mats Jonasson, Jonas Sjöberg, "Optimal Braking and Steering Control Under Split Friction on Curved Roads". Published in *Lecture Notes in Mechanical Engineering*, 2024, `https://doi.org/10.1007/978-3-031-70392-8_85`.

[D] **Ektor Karyotakis**, Mats Jonasson, Derong Yang, "Trajectory Optimization for Safe Stops with Laterally Varying Road Friction Ahead". Submitted to *IEEE T-ITS*, in March 2025.

Other publications by the author, not included in this thesis, are:

[E] **Ektor Karyotakis**, Mats Jonasson, Derong Yang, Jonas Sjöberg, "Minimizing Stopping Distance on Split Friction via Steering and Individual Wheel Braking Optimization". In: Huang, W., Ahmadian, M. (eds) Advances in Dynamics of Vehicles on Roads and Tracks III. IAVSD 2023. *Lecture Notes in Mechanical Engineering*. Springer, Cham. `https://doi.org/10.1007/978-3-031-66968-2_37`.

[F] **Ektor Karyotakis**, Derong Yang, Mats Jonasson, Jonas Sjöberg, "Method for determining a braking distance estimate for a vehicle, method for operating a driver assistance system of a vehicle, data processing apparatus and computer program". Patent granted (EP4342749B1), Nov. 2024.

Contents

Acknowledgments

First and foremost, I would like to extend my heartfelt gratitude to my supervisors, Derong Yang, Mats Jonasson, and Jonas Sjöberg, for their invaluable guidance and mentorship throughout the first half of my PhD journey. Our countless hours of discussions and even debates about the direction of my research have significantly contributed to my growth as a researcher.

To my unwavering supporter, my rock, and my source of joy, Alexandra—this journey would not have been possible without your steadfast presence and encouragement. I am deeply grateful for your patience, your constant support, and the countless ways you have enriched my life.

Finally, I would like to acknowledge: (a) Volvo Car Group (Volvo Cars) and (b) Fordonsstrategisk forskning och innovation (FFI) [Strategic Vehicle Research and Innovation] part of Verket för Innovationssystem (VINNOVA) [Swedish Innovation Agency], for funding this project (Vehicle Motion Control Using Data-Driven Varying Road Friction Map; 2020-05169).

Acronyms

ABS:	Anti-lock Braking System
ACC:	Adaptive Cruise Control
ADAS:	Advanced Driver Assistance System
AEB:	Automated Emergency Braking
CoG:	Centre of Gravity
DT:	Double-Track (Model)
ESB:	Emergency Steering and Braking
ESC:	Electronic Stability Control
FCD:	Floating Car Data
LKA:	Lane Keeping Aid

NHTSA:	National Highway Traffic Safety Administration
OCP:	Optimal Control Problem
PM:	Particle Model
RLS:	Recursive Least Squares
RSC:	Road Surface Condition
ST:	Single-Track (Model)
V2X:	Vehicle-to-Everything

Part I

Overview

CHAPTER 1

Introduction

1.1 Background

The push to make vehicles autonomous is driving significant advancements in automotive technology. As vehicles become smarter and more software-oriented, they offer increased functionality and enhanced capabilities. A key aspect of this evolution is the data-driven approach, where vehicle fleets collect and send data to the cloud. Companies like NIRA Dynamics and Volvo Cars are at the forefront, gathering road condition and surface information and projecting it onto online maps. This data can be used by traffic authorities to better maintain roads during winter and to warn other drivers (see Fig. 1.1). The advent of vehicle-to-everything (V2X) communication promises even more information, enabling interconnected vehicles to dynamically adapt to changing conditions. However, a critical challenge remains: the vehicle's motion capability is largely dependent on the road surface conditions. This issue is often overlooked due to the *high uncertainty* of road friction estimates and their *low availability*.

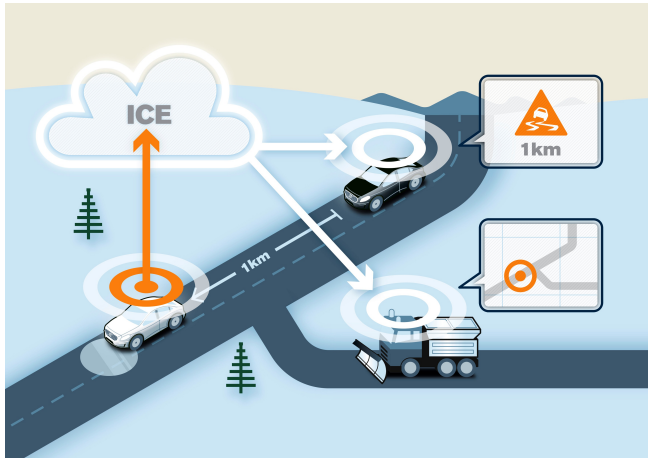

Figure 1.1: Slippery road warning shared with other cars [1]

1.2 Crash statistics

Most drivers know that there is an increased accident risk in poor road and weather conditions. This is well documented in literature, typically proved after analyzing data from crash databases. One commonly used open database is the Fatality Analysis Reporting System (FARS) from the National Highway Traffic Safety Administration (NHTSA) of the USA. Using this database, [2] showed a positive trend in reducing fatalities due to adverse road conditions over 1994-2012, coinciding with the general trend of reducing accidents as vehicles become smarter and authorities maintain the roads better. This newer study [3] showed that accident risk significantly increases in rare adverse road and weather conditions, namely icy rain, slush, and combinations that make the pavement slippery, e.g., heavy snowfall and below freezing temperatures.

The same study also found a higher risk for single-vehicle accidents. These are typically crashes with the infrastructure after a road departure. One of the pre-impact mechanics in such accidents is typically skidding, where a vehicle becomes unstable after braking or steering just before the crash. Skidding happens more frequently on low-friction conditions [4]. The role of skidding in crashes can be analyzed based on road surface conditions using NHTSA's online database querying tool [5], with the results presented in Table 1.1. Road

Table 1.1: Subset of all vehicles involved in fatal crashes with query pre-impact skidding, per crash year and road surface condition (adapted from *Paper D*).

	Roadway Surface Conditions				
Crash Year	Dry	Wet	Snow	Slush	Ice
2020	3906	830	60	30	153
2021	3918	770	78	20	185
2022	3927	651	89	34	202
Total	11751	2251	227	84	540
Percentage of total	7,9%	11,9%	21,8%	30,5%	35,7%

surface conditions are ranked from high to low friction in the table (typical ranges can be found in [6], *Paper A*). A clear trend emerges: lower friction correlates with a higher percentage of fatal accidents involving pre-impact skidding. This suggests current stability systems can be further improved, but also highlights the potential for reducing these accidents by incorporating predictive road friction information in vehicle motion planning.

Automation has led to a reduction in accident risk, except for comfort-related functions such as the adaptive cruise control (ACC), which increase the risk instead, as analyzed in [7]. Specifically, lane-keeping aid (LKA), driver monitoring systems (DMS), and automated emergency braking (AEB) showed the strongest crash rate reduction effects. The LKA reduced crash rates by 19.1%, while AEB achieved a 10.7% reduction. Incorporating friction information can further enhance safety, as discussed in the following section.

1.3 Road Condition and Friction Estimation

Tyre-road interaction plays a critical role in vehicle behavior, with the friction limit determining the maximum achievable braking and steering forces. In conventional human-driven vehicles, drivers rely on experience and intuition to anticipate how the vehicle will respond to road conditions. While human drivers often perform well, many accidents still result from misjudging the situation—such as entering a curve at excessive speed or failing to brake hard enough.

To enhance safety and support driver decision-making, Advanced Driver Assistance Systems (ADAS) have been developed. Systems like Anti-lock Braking System (ABS) and Electronic Stability Control (ESC) operate effectively even without explicit road friction knowledge. However, the performance of many other ADAS functions is heavily influenced by the available road friction, which is typically not included in their design.

Common assumptions about the road condition

Optimal conditions

The basis for current in-production ADAS is to assume that the road surface is dry asphalt, and the temperature is well-above zero. ADAS are designed to operate under these road conditions mainly due to legal reasons and the need to minimize false interventions [8]. Studies, both theoretical and experimental, have shown that most ADAS are less effective in adverse weather conditions. Real-life tests of an AEB system in optimal and adverse conditions [9] revealed significant variations in detection distance and braking initiation. This reduced effectiveness in adverse weather is partly due to sensor performance deterioration [10].

Homogeneity assumption

Another common assumption in the literature is that road friction remains constant based on the last observed value. The homogeneity assumption has two implications.

First, using the tyre as a sensor, obtaining frequent and accurate estimates typically requires *significant tyre excitation*, coming from either braking or steering. The required level of excitation is estimated to lie in the range 30–50% of the maximum tyre force [11]. Such estimation will be referred to as *local friction estimation*, as it only provides the current friction coefficient under the tyres. In contrast, *predictive friction estimation* refers to information about road conditions ahead of the vehicle, which can be obtained from cloud data or perception sensors.

Second, there might be *local variations* of the road surface *ahead* of the vehicle. This study [12] examined the variations in road surface temperature and condition from traffic camera images. They discovered differences in temperature and condition laterally across the road, which were more pronounced in

low-traffic areas like the hard shoulder. One explanation for these variations is differential drying, which is caused by the traffic clearing contamination such as water or snow as drivers follow similar routes.

Addressing these limitations requires dynamically estimating and adapting to varying road conditions.

Road friction estimation

Accurate road friction estimation is crucial for ADAS, as it enables precise calculations based on the friction limit. This section introduces current and emerging technologies for estimating road friction, and discusses their primary benefits and limitations.

Tyre-based

Local friction estimation using tyres as sensors has been researched for over three decades, yet it remains largely an open question. The most common methods are slip-based, relying on measuring tyre slip during either longitudinal excitation (braking or accelerating) [13], [14] or lateral excitation (steering). The measured slip data are then fitted to a tyre/friction model using methods like recursive least squares (RLS) [15], [16] or newer approaches like neural networks [17].

The widely used slip slope method [13], [14], [16] focuses on the linear tyre region (tyre stiffness), assuming that knowing the initial slope allows for estimating the maximum friction coefficient μ (see Fig. 1.2). However, the slip slope method is highly variable due to factors like tyre pressure, wear [13], [14], and temperature [11]. This method typically involves low tyre excitation. With higher excitation, a more advanced tyre model can be utilized. *Paper B* applied the method from [15], which is effective at maximum braking. Only a few samples of the linearized RLS algorithm near the maximum are needed to obtain the friction coefficient with high accuracy.

Due to the low-excitation problem and the difficulty of accurate friction estimation, active excitation algorithms have been developed. In [18], one axle is driven while the other brakes, resulting in zero net force but still exciting the tyres. With a fleet of vehicles, active excitation (probing) can be requested from an available vehicle at a specified location [19].

Another promising area is equipping tyres with additional sensors, such as

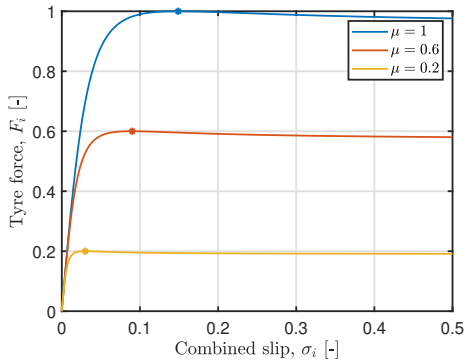

Figure 1.2: Normalized tyre force-slip curves on various road frictions. The peak is marked with an asterisk, with its magnitude corresponding to the road friction coefficient μ and its position to the peak slip per tyre σ_i^* (*Paper B*).

acceleration sensors and RFID [20]. These intelligent tyres offer new computational opportunities for tyre manufacturers, enabling new services for tyre wear and friction estimation, among others.

Perception-based road condition estimation

Perception-based sensors, such as cameras and lidars, are increasingly being incorporated into passenger vehicles due to their preview information and high availability. For road friction estimation, though, mapping images to road friction coefficient values is challenging. Instead, the road surface condition (RSC) (e.g., dry, wet, or snow) can be estimated. Most papers classify the entire road image [21], [22], while others focus on dividing the image into grids of the drivable area ahead of the vehicle [23], [24], which is more useful for planning the vehicle's motion. The overall confidence of such algorithms typically exceeds 90% for whole image RSC. For grid-based RSC, by incorporating the whole image and temperature measurements, the confidence can reach up to about 90% [24], depending on the available data and number of classes selected.

This study [22] demonstrated that using RSC to update the reference slip of a ABS logic has the potential to reduce braking distances on non-dry roads.

Similarly, [25] highlighted the significant benefits of fusing RSC with local friction estimation obtained during braking, showing enhanced performance in several simulated critical scenarios. Combining these two estimates can leverage both the predictive capabilities of a perception system and the high accuracy of tyre excitation. As perception-based estimation continues to advance, the potential for integrating RSC with additional ADAS is expected to increase.

Cloud road friction data

A promising area of business involves collecting floating car data (FCD), such as road condition, friction, and roughness, using fleets of vehicles. Some companies equip their vehicles with additional sensors, like optical sensors [26], while others rely solely on onboard estimation. The data are then uploaded to the cloud and projected onto online maps. By providing real-time information on road conditions, traffic authorities can respond more quickly to hazards and plan maintenance more effectively.

In [27], the authors analyzed FCD during the winters of 2021-2022 in Sweden. They demonstrated the promising reliability of real-time data compared to friction test measurements and compared friction data suppliers to each other. They also claimed sufficient coverage of the Swedish road network for winter road maintenance understanding and follow-up.

Real-time road information can also provide warnings to drivers, as in Volvo Cars' Slippery Road Alert [1] (as shown in Fig. 1.1), or even use this information to plan the vehicle's motion (*Paper D*). In his thesis, [28] investigated the potential of a weather-related road surface condition estimator from FCD to enhance current ADAS, such as adaptive cruise control (ACC) and emergency steering and braking (ESB) systems. Knowing the current road condition allows for increasing the safety distance for ACC and adjusting the points to brake and steer of ESB more accurately. However, to make these adjustments, a road friction value must be assigned to each road condition, which may still be inaccurate.

The sensitivity of road friction misidentification has been investigated by TU Braunschweig [29] for an AEB system [30] and an emergency steering system [31]. Mistaking a high-friction surface for a low-friction one (false positive) can lead to unnecessary interventions and driver frustration. Conversely, mistaking a low-friction surface for a high-friction one (false negative)

is safety-critical.

Although cloud data offer great potential, challenges remain, such as ensuring data accuracy, managing large volumes of data, and addressing privacy concerns. Continued advancements in sensor technology and data processing will be crucial in overcoming these obstacles and fully realizing the potential of cloud-based road friction data.

1.4 Contributions

The previous sections established the common assumptions and limitations of current ADAS with regard to road friction and introduced the prospects of predictive road friction information. This thesis addresses one of the most immediate aspects of using predictive road friction information: improving the braking performance. This is achieved by:

- Establishing methods to find the shortest braking distance on roads with varying friction conditions.
- Analyzing the combined braking and steering mechanics under those conditions.
- Proposing control frameworks that enable reaching the shortest braking distance.

Paper-specific contributions:

- **Paper A**:
  - Natural road friction variation can remain minimal with proper test-track preparations and post-processing methods.
  - Local road friction variations can still occur despite test-track preparations.
- **Paper B**:
  - Imposing a slip constraint on a low-friction tyre reduces the total braking potential (Section 4.1).
  - Analysis of the physical limits of combined steering and braking on split friction roads (Sections 4.2-4.3 and Fig. 13).

  - Significant reductions in braking distance can be achieved through automated steering compared to human drivers (Section 7.1).

- **Paper C**:
  - Extension of braking & steering optimization from *Paper B* to curved paths.
  - Low friction on the inner curve side is detrimental to safety due to load transfer to the outer side.

- **Paper D**:
  - Formulation of an optimal control problem that considers lateral variations in road friction for calculating the shortest braking distance.
  - Development of a particle model that provides near-optimal braking paths for varying road friction profiles.

1.5 Limitations

The scope of this study is limited to:

- The vehicle operates on flat, asphalted roads. Off-road terrains are not considered.
- The tyre-road interaction is simplified by neglecting texture-related effects such as snow or gravel displacement. Instead, road friction is assumed to be uniform across each tyre contact patch but may vary between different road sections.

CHAPTER 2

Vehicle Models

Vehicle dynamics describe how a vehicle behaves as a dynamical system over time, encompassing acceleration, braking, and steering. A precise understanding of these dynamics is essential for developing effective automotive control systems.

This thesis focuses on the vehicle's interaction with road friction, requiring a curvilinear coordinate frame. Unlike a time-based reference, a curvilinear frame relates vehicle motion to the distance along the path centerline, making it particularly useful for optimization problems involving road friction variations.

The vehicle models developed in this thesis incorporate the following key aspects:

- **Longitudinal Dynamics** – Governs acceleration and braking forces along the path. A crucial component is ABS, which regulates wheel slip to achieve maximum braking force.

- **Lateral Dynamics** – Describes motion perpendicular to the path, including steering and yaw disturbances. While ESC influences lateral stability, it is not modeled in this thesis.

- **Curvilinear Frame** – Captures path curvature and variations in road friction along the trajectory.
- **Road-Tyre Interaction** – Models frictional forces between the tyres and road surface, which are critical for braking performance on different road conditions.

Accurate modeling of these aspects is essential for optimizing braking and friction-based path-planning. The main methodology of this study is optimization. A standard optimal control problem (OCP) formulation minimizes a cost function J as

$$\begin{array}{lll} \min & J & : \text{cost} \\ \text{subject to} & \dot{\boldsymbol{x}} = f(x,u) & : \text{dynamics} \\ & g(x,u) = 0 & \\ & h(x,u) \leq 0 & : \text{constraints} \end{array} \tag{2.1}$$

The key components of this formulation are:

- **Cost (J)**: The objective function to be minimized, such as braking distance (*Paper D*) or static acceleration (*Papers B, C*).
- **Dynamics ($\dot{\boldsymbol{x}} = f(x,u)$)**: The vehicle model, which in this thesis includes:
  - Vehicle position and orientation.
  - Forces and moments acting at the center of gravity.
  - Tyre forces and their interaction with the road.
  - Actuator dynamics, if relevant.
- **Constraints ($g(x,u) = 0,\ h(x,u) \leq 0$)**: These enforce physical and operational limits, such as:
  - Actuator constraints (e.g., steering angle or brake torque limits).
  - Physical constraints (e.g., slip limits, tyre friction limits).
  - Road constraints (e.g., lane boundaries).

The following sections introduce the vehicle models used in this thesis, progressing from simplified to more complex representations.

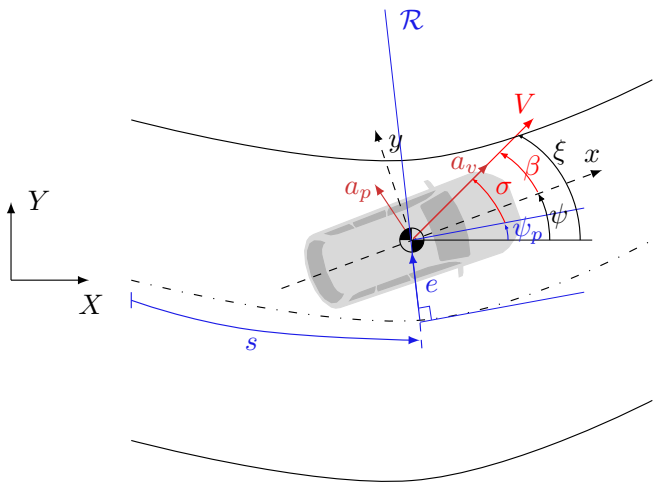

Figure 2.1: Vehicle position, velocity, and orientation in the inertial coordinate frame XY and in the curvilinear coordinate frame se defined by the path centerline. The elapsed centerline distance s and the lateral distance e of frame se are denoted with blue color, at a curve radius $\mathcal{R}$. The velocity vector V, its corresponding angles, and the acceleration components along, a_v, and perpendicular, a_p, to V are denoted with red color (*Paper D*).

2.1 Vehicle Position and Orientation in a Curvilinear Frame

The following derivation is based on the formulations presented in *Paper D*.

The vehicle's motion is described in a curvilinear coordinate frame aligned with the path centerline, as shown in Fig. 2.1, [32]. This choice is motivated by the need to relate the road friction profile to position along the path rather than time, useful for the coming optimization problems.

At the traveled distance $s(t)$ [m] along the path centerline, the path's curvature is $\kappa = 1/\mathcal{R}$ [1/m], where $\mathcal{R}$ is the radius of curvature. The vehicle's lateral deviation from the centerline is e [m], with the center of gravity chosen as the reference point for straightforward coordinate transformations.

The vehicle's orientation is characterized by several angles: the path centerline orientation ψ_p [rad], the vehicle's yaw angle ψ [rad], and the velocity vector orientation σ [rad] relative to the path. Additionally, β [rad] represents the body slip angle, and ξ [rad] is the course angle relative to the inertial frame XY. The velocity magnitude is given by V [m/s].

The course angle ξ determines the inertial position of the vehicle

$$\begin{aligned} \dot{X} &= V\cos(\xi), \\ \dot{Y} &= V\sin(\xi). \end{aligned} \tag{2.2}$$

From Fig. 2.1, ξ is expressed as

$$\xi = \sigma + \psi_p, \tag{2.3}$$

$$\xi = \beta + \psi. \tag{2.4}$$

Assuming circular motion, the centerline yaw rate follows

$$\dot{\psi}_p = \kappa \dot{s}. \tag{2.5}$$

Differentiating (2.3) and using (2.5) gives

$$\dot{\xi} = \dot{\sigma} + \kappa \dot{s}. \tag{2.6}$$

Similarly, differentiating (2.4) yields

$$\dot{\beta} = \dot{\xi} - \dot{\psi}. \tag{2.7}$$

This links the yaw rate $\dot{\psi}$ [rad/s] to the body slip angle rate $\dot{\beta}$ [rad/s].

Change of independent variable

With the vehicle's position and orientation defined, we express velocity along s to change the independent variable from time to space, simplifying the incorporation of road friction variations. From Fig. 2.1, this transformation follows as

$$S_p = \frac{dt}{ds} = \frac{1 - \kappa e}{V\cos(\sigma)}. \tag{2.8}$$

The state derivatives in space coordinates are then given by a transformation of the time derivatives as

$$\frac{d\boldsymbol{x}(s)}{ds} = \frac{d\boldsymbol{x}(t)}{dt} S_p. \tag{2.9}$$

Further details are available in *Paper D* and [32].

2.2 The Particle Model

This section follows the formulation in *Paper D*, where the particle model serves as a baseline for trajectory optimization.

A simplified vehicle representation, the particle model (PM), assumes all mass is concentrated at the center of gravity without inertia. Despite its simplicity, the PM provides near-optimal paths compared to high-fidelity models, while significantly reducing computational complexity.

From Fig. 2.1, Eqs. (2.6), (2.8), and [33], the particle dynamics in the curvilinear coordinate frame are given by

$$\begin{aligned} \dot{e} &= V \sin(\sigma), \\ \dot{\sigma} &= \dot{\xi} - \kappa / S_p, \\ \dot{V} &= a_v - k_d V^2, \\ \dot{\xi} &= \frac{a_p}{V}, \end{aligned} \tag{2.10}$$

where k_d is the aerodynamic coefficient modeling the drag force acting on the vehicle. The acceleration components are expressed along the velocity vector V, with a_v [m/s^2] denoting the tangential (longitudinal) component and a_p [m/s^2] the radial (lateral) component. The above nonlinear system has the state vector $\boldsymbol{x} = \begin{bmatrix} e & \sigma & V & \xi \end{bmatrix}^\mathsf{T}$, and the input vector $\boldsymbol{u} = \begin{bmatrix} a_v & a_p \end{bmatrix}^\mathsf{T}$.

Friction limits

A key simplification of the particle model is that it neglects tyre mechanics. Instead, the acceleration components are constrained by the friction ellipse

$$\left(\frac{a_v}{k_{el}} \right)^2 + a_p^2 \leq (\mu(s, e)\, g)^2, \tag{2.11}$$

where k_{el} is an ellipse parameter representing the proportion of longitudinal to lateral friction potential. The road friction coefficient $\mu(s, e)$ varies with position $[s, e]$ along the path, affecting the local acceleration limits. Consequently, minimizing the braking distance depends on the local road properties.

Next, we introduce more advanced vehicle models that model the tyre-road interaction.

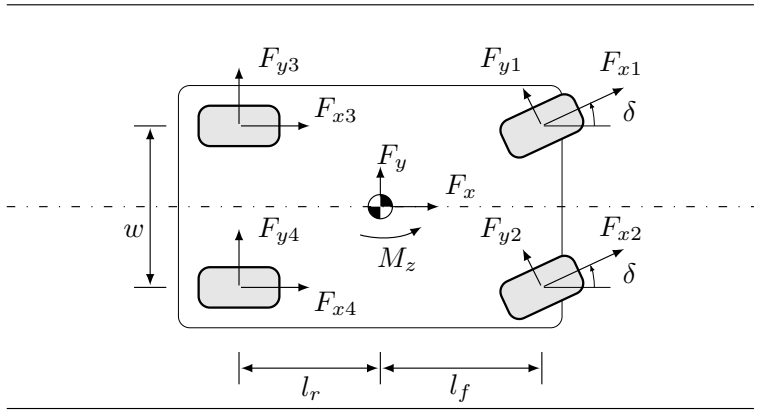

Figure 2.2: Double-track vehicle model with front-wheel steering (*Paper B*).

2.3 Tyre-Based Vehicle Modeling

This section presents two vehicle models: the single-track model (ST) and the double-track model (DT). The ST is a simplified version of the DT, obtained by lumping the forces on each axle together. The ST was used as a benchmark for trajectory optimization of the particle model in *Paper D*, while the DT was employed for static optimization in *Paper B*.

The section is structured as follows: first, it introduces the total forces and moments at the center of gravity (CoG) and their relation to the vehicle states. Next, it details how these forces are distributed among the tyres in each vehicle model. Finally, it discusses the friction constraints that limit the tyre forces.

Figure 2.2 illustrates the vehicle model notation and tyre forces. The total force at the CoG, denoted as F [N], is decomposed into longitudinal (F_x) and lateral (F_y) components. The yaw moment is M_z [Nm] and the steering angle δ [rad]. The force components and yaw moment are expressed as a function of the body accelerations $[a_x, a_y]$ [m/s^2] and yaw acceleration $\ddot{\psi}$ [rad/s^2] from

Newton's second law as

$$a_x = \frac{F_x}{m}, \tag{2.12}$$

$$a_y = \frac{F_y}{m}, \tag{2.13}$$

$$\ddot{\psi} = \frac{M_z}{I_{zz}}, \tag{2.14}$$

with m the vehicle mass [kg] and I_{zz} the rotational inertia [$\mathrm{kg\,m^2}$]. The equations governing F_x, F_y, and M_z are provided in Section 2.3 for the single-track model and Section 2.3 for the double-track model.

The body accelerations are mapped to a_v and a_p using the transformation

$$\begin{bmatrix} a_v \\ a_p \end{bmatrix} = R(\beta) \begin{bmatrix} a_x \\ a_y \end{bmatrix}, \tag{2.15}$$

where $R(\cdot)$ is the rotation matrix. For an angle ϕ, the rotation matrix is defined as

$$R(\phi) = \begin{bmatrix} \cos(\phi) & -\sin(\phi) \\ \sin(\phi) & \cos(\phi) \end{bmatrix} \tag{2.16}$$

Using the above acceleration components (2.15), the yaw torque from (2.14), and the angular expression (2.7), the particle dynamics in (2.10) are adapted for the single-track and double-track models as

$$\begin{aligned} \dot{e} &= V \sin(\sigma), \\ \dot{\sigma} &= \frac{a_p}{V} - \kappa / S_p, \\ \dot{V} &= a_v - k_d V^2, \\ \dot{\beta} &= \frac{a_p}{V} - \dot{\psi}, \\ \ddot{\psi} &= \frac{1}{I_{zz}} M_z, \end{aligned} \tag{2.17}$$

which has the state vector $\boldsymbol{x} = \begin{bmatrix} e & \sigma & V & \beta & \psi \end{bmatrix}^\intercal$, and the input vector $\boldsymbol{u} = \begin{bmatrix} F_{xi} & \delta \end{bmatrix}^\intercal$. The input formulation follows from the fact that the acceleration components will be expressed as functions of the longitudinal tyre forces F_{xi} and the steering angle δ, i.e., $a_{\{v,p\}} = a_{\{v,p\}}(F_{xi}, \delta)$, as presented in the coming sections.

The single-track model

For the single-track (ST) model, the forces F_x and F_y and the yaw moment M_z about the vertical axis are given by

$$a_x = \frac{1}{m}(-F_{yf}\sin(\delta) + F_{xf}\cos(\delta) + F_{xr}), \tag{2.18}$$

$$a_y = \frac{1}{m}(F_{yf}\cos(\delta) + F_{xf}\sin(\delta) + F_{yr}), \tag{2.19}$$

$$M_z = l_f(F_{yf}\cos(\delta) + F_{xf}\sin(\delta)) - l_r F_{yr}, \tag{2.20}$$

with the front longitudinal force F_{xf} [N], rear longitudinal force F_{xr} [N], and steering angle δ as the vehicle inputs. The lateral forces F_{yf} [N] and F_{yr} [N] are expressed as functions of the states through the chosen tyre model.

The double-track model

For the double-track (DT) model, the forces and moments become

$$\begin{aligned} F_x &= (F_{x1} + F_{x2})\cos\delta - (F_{y1} + F_{y2})\sin\delta + F_{x3} + F_{x4}, \\ &\approx (F_{x1} + F_{x2} + F_{x3} + F_{x4}) - (F_{y1} + F_{y2})\,\delta, \end{aligned} \tag{2.21}$$

$$\begin{aligned} F_y &= (F_{x1} + F_{x2})\sin\delta + (F_{y1} + F_{y2})\cos\delta + F_{y3} + F_{y4}, \\ &\approx (F_{y1} + F_{y2} + F_{y3} + F_{y4}) + (F_{x1} + F_{x2})\,\delta, \end{aligned} \tag{2.22}$$

$$\begin{aligned} M_z &= ((F_{x1} + F_{x2})\sin\delta + (F_{y1} + F_{y2})\cos\delta)\cdot l_f \\ &\quad - (F_{y3} + F_{y4})\cdot l_r \\ &\quad + ((-F_{x1} + F_{x2})\cos\delta + (F_{y1} - F_{y2})\sin\delta - F_{x3} + F_{x4})\cdot \frac{w}{2} \\ &\approx M_\delta - M_{\Delta F_x} + M_{cross}, \end{aligned} \tag{2.23}$$

where a small δ assumption is used. F_i [N] refers to the four tyre forces $i \in \{1, 2, 3, 4\}$, with F_{xi} the longitudinal and F_{yi} the lateral ones. $[l_f, l_r, w]$ [m] are length components defined in Fig. 2.2. The vehicle inputs here are F_{xi} and δ. The terms $[M_{\Delta F_x}, M_\delta, M_{cross}]$ are yaw torque contributions due

to braking, steering, and a cross-term, respectively, given by

$$M_{\Delta F_x} = ((F_{x1} + F_{x3}) - (F_{x2} + F_{x4}))\frac{w}{2}, \tag{2.24}$$

$$M_{\delta} = (F_{y1} + F_{y2})l_f - (F_{y3} + F_{y4})l_r, \tag{2.25}$$

$$\begin{aligned} M_{cross} &= (F_{x1} + F_{x2})l_f\,\delta + (F_{y1} - F_{y2})\frac{w}{2}\,\delta \\ &\approx (F_{x1} + F_{x2})l_f\,\delta. \end{aligned} \tag{2.26}$$

The forces $[F_x, F_y]$ and moments M_z on the CoG are obtained through the four tyres, briefly explained below.

Tyre modeling

The tyre forces are typically modeled as functions of slip, with lateral forces being a function of the steering angle δ. Different approaches exist for modeling the combined effects of braking and steering: *Paper B* employed a combined slip model incorporating both longitudinal and lateral slips, whereas *Paper D* used a simplified approach that limits the maximum lateral force, following [34]. For a more detailed discussion on tyre force-slip relationships, refer to the corresponding papers and [16], [35]–[37].

In this work a simplified Pacejka model [35] was used, defined as

$$F_i = F_{\max,i} \sin\left[B \arctan\left(\frac{C_i \sigma_i}{B\, F_{\max,i}}\right)\right], \tag{2.27}$$

where C_i are the tyre stiffness, B is a shape factor at large slip, and $F_{\max,i}$ are the maximum attainable forces, defined as

$$F_{\max,i} = \mu_i(s, e) F_{zi}, \tag{2.28}$$

with μ_i the friction coefficient in the curvilinear frame se and F_{zi} the vertical force of each tyre. The F_{zi} are obtained from a steady state longitudinal and lateral load transfer model, as in [38, p. 350]. Further, C_i is assumed to be linearly dependent on F_{zi}. The tyre force F_i as a function of the combined slip σ_i is presented in Fig. 1.2 and shows how the curve changes with the friction coefficient μ. In the figure, the asterisks depict the $F_{\max,i}$, which happens at the *peak slip*.

The friction circle limitation is defined as

$$F_{yi}^2 + (F_{xi}/k_{el})^2 \leq (F_{\max,i})^2\,. \tag{2.29}$$

CHAPTER 3

Braking and Optimization Approaches

This chapter begins by discussing existing solutions for maximum braking, their underlying principles, and their limitations. A key drawback of current systems, such as ABS and ESC, is their reactive nature—they respond only to the vehicle's current state. However, many accidents could be mitigated or even prevented if corrective actions were taken earlier. This can be achieved by incorporating information about the vehicle's surroundings, such as nearby traffic and road conditions, to predict its motion and intervene proactively when necessary. The chapter then introduces our proposed solutions for instantaneous control on split friction roads, where ABS and ESC may be suboptimal, as well as cases where predictive friction information is essential for minimizing stopping distance through full-trajectory optimization.

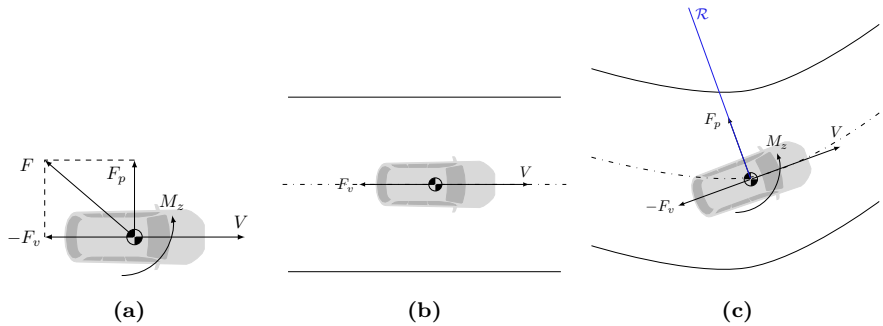

Figure 3.1: Vehicle velocity vector V, force vector F projected F_v along and F_p perpendicular to V, and yaw torque M_z for: (a) General case, (b) Straight uniform road, (c) Curved road.

3.1 Maximizing Braking Force: Problem Formulation

As introduced in Section 2.1, a road vehicle's trajectory is characterized by its velocity vector V, the total force F, and the yaw torque M_z acting on its CoG, as illustrated in Fig. 3.1a. Figure 3.1b presents a simplified case of a straight road with uniform friction, while Fig. 3.1c depicts the vehicle on a curved road.

Each scenario is discussed in the following sections:

- Section 3.2 considers braking on a straight road with uniform friction, representing a simplified yet insightful baseline scenario.
- Section 3.3 introduces the special case of split friction, where one side of the vehicle experiences low friction while the other remains on high friction.
- Section 3.3 addresses path planning for braking on roads with both longitudinal and lateral friction variations.

Using a force-centric approach (as in [36]), the following theorem gives the shortest braking distance, when the road friction profile only changes in the longitudinal direction (along the vehicle travel, but not perpendicular to it):

Theorem 1: *On laterally uniform road friction roads, the shortest braking distance is obtained by maximizing the force opposite to the velocity, F_v, at every time instant.*

The theorem can be expressed as an optimization problem as

$$\begin{aligned} \max_{t} \quad & -F_v(t) \quad \forall t, \\ \text{subject to} \quad & F_p, \\ & M_z, \end{aligned} \tag{3.1}$$

which is essentially an instantaneous optimization problem. When the road friction profile is uniform across the lane (i.e., no lateral variation), there is no reason for the vehicle to deviate from the path centerline. In such cases, the instantaneous solution converges to the full-trajectory solution, as the optimal path remains along the centerline. However, as shown in *Paper D*, when the friction profile varies laterally, simply maximizing the force opposite to the direction of travel at each instant can become suboptimal. In these scenarios, planning the entire braking trajectory—rather than reacting moment-to-moment—can result in a significantly shorter braking distance.

From (3.1), braking on a straight path can be summed up to

$$\begin{aligned} \max_{t} \quad & -F_v(t) \quad \forall t, \\ \text{subject to} \quad & F_p(t) \to 0, \\ & M_z(t) \to 0, \end{aligned} \tag{3.2}$$

while braking on a non-straight path to

$$\begin{aligned} \max_{t} \quad & -F_v(t) \quad \forall t, \\ \text{subject to} \quad & F_p(t) \to F_{pd}(t), \\ & M_z(t) \to M_{zpd}(t), \end{aligned} \tag{3.3}$$

where F_{pd} and M_{zd} are the desired perpendicular force and yaw torque. In the special case of braking on a split friction road, following a straight path is determined by (3.2) (*Paper B*). For curved roads, an instantaneous solution is derived by setting $F_{pd}(t) = m\frac{V(t)^2}{R(t)}$ and $M_{zpd} = 0$ (*Paper C*). Otherwise, F_{pd} and M_{zd} can be indirectly determined by following a desired path.

The optimization problems (3.1)-(3.3) are presented at a high level. Real vehicle actuation originates from its brakes, powertrain, and steering system, all of which are transmitted through the tyres and the tyre-road interaction.

Consequently, the actual reconstruction of the high-level forces F_v, F_p, and M_z is ultimately a combination of tyre forces, steering angles, and vehicle states. This interaction is explained in the vehicle models of Chapter 2. Braking on a straight path with uniform road friction can greatly reduce the complexity of the vehicle model, as discussed in the next section.

3.2 Braking Distance on Uniform Roads

It is commonly assumed that braking occurs in a relatively straight line and that the road conditions remain nearly uniform, as illustrated in Fig. 3.1b. In this context, "uniform" refers to the assumption that friction is constant or only varies slowly over the braking path. The uniformity holds in an averaged sense, such that the road friction coefficient can be treated as constant over the braking distance. Under such conditions, any steering interventions are minimal, allowing the braking distance calculations to be simplified accordingly.

Mathematically, these assumptions can be expressed relative to the general optimization problem (3.1) as $\{F_p = 0, M_z = 0, F = F_v\}$. The total force on the vehicle F is opposite to the path, as illustrated in Fig. 3.2. Using energy conservation, the following relation holds

$$\int_{P_0}^{P_1} F \, ds = \frac{1}{2} m \, V_1^2 - \frac{1}{2} m \, V_0^2, \tag{3.4}$$

where $P_0,\ P_1$ are the starting and final braking points, and $V_0,\ V_1$ the starting and final velocities; m is the vehicle's mass.

For uniform friction and maximum F at every instant, the braking distance s becomes from the above

$$\begin{aligned} \int_{P_0}^{P_1} (-m \, \mu \, g) \, ds &= \frac{1}{2} m \, V_1^2 - \frac{1}{2} m \, V_0^2, \\ \Rightarrow \mu \, g \, s &= \frac{1}{2} \left(V_0^2 - V_1^2 \right), \\ \Rightarrow s &= \frac{V_0^2 - V_1^2}{2 \, \mu \, g}, \end{aligned} \tag{3.5}$$

which shows that the braking distance is a function of the road friction coefficient μ and the initial speed V_0; g is the gravitational constant.

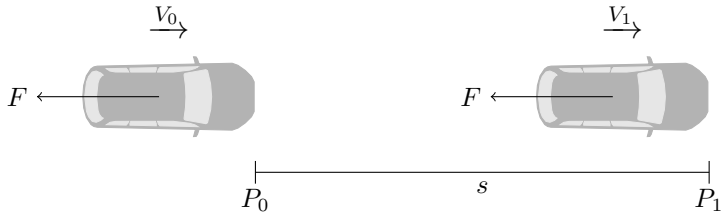

Figure 3.2: A vehicle braking in a straight line on a straight path, with uniform friction (same setting as Fig. 3.1b). s is the braking distance, $[P_0, V_0]$ are the starting braking point and velocity, and $[P_1, V_1]$ the final braking point and velocity.

Although variations in friction may occur along the braking path, the equation (3.5) is still applicable when considering the *average friction* $\bar{\mu}$ over the braking distance, which is defined as

$$\bar{\mu} = \frac{1}{P_1 - P_0} \int_{P_0}^{P_1} \mu(s)\, ds. \tag{3.6}$$

Thus, in this section, the friction is treated in a macroscopic sense, with $\mu = \bar{\mu}$.

While this approach works well for theoretical calculations, it is impractical for real-world applications such as onboard predictive friction estimates, where friction is often discretized along the path ahead. To handle this, a piecewise constant distance calculation algorithm is required, such as the one patented in *Patent F*.

Tyre-road interaction

A key assumption in deriving (3.5) is that maximum braking is achieved at every instant, as stated in Theorem 1. This is facilitated by ABS.

ABS primarily prevents wheel lock-up, maintaining directional control. Its secondary function is to sustain high braking forces by dynamically identifying the *peak slip*—the slip ratio that maximizes tyre force, as shown in Fig. 1.2. Notably, this approach does not require prior friction knowledge. In practice, production ABS operates through a complex multi-phase regulation, with up to eight phases [39]. The effectiveness of the ABS on different surfaces and speeds can be found in [40], [41].

Since each wheel has independent ABS actuation, maximum force can be achieved per tyre, maximizing braking for the whole vehicle. Under uniform lateral friction conditions, this would also result in the shortest braking distance. However, as described in *Paper B*, when friction varies significantly between the vehicle's sides, achieving peak slip on all wheels may be infeasible due to the induced yaw moment on the vehicle. This finding is explained in Section 4.3.

Autonomous Emergency Braking

Autonomous Emergency Braking (AEB) is an ADAS designed to prevent or mitigate collisions by automatically applying the vehicle's brakes when an imminent collision is detected. The system utilizes various sensors, such as radar, LiDAR, and cameras, to monitor the vehicle's surroundings and assess potential collision threats. Since its initial introduction, AEB systems have undergone significant advancements. Early systems were primarily designed to operate at low speeds, suitable for urban environments. Modern AEB systems have expanded their capabilities to include high-speed scenarios, pedestrian detection, and rear automatic emergency braking. More details on current AEB technologies and other ADAS features included in Volvo's Safe Space can be found in [42].

In an AEB system, the safe distance is first estimated (typically using (3.5)) and then compared to the measured distance to the front vehicle. Thus, its effectiveness relies on accurately assessing the road condition. Correct safe distance estimation is crucial, as overestimating distance can delay braking, endangering the vehicle and others, while underestimation may cause unnecessary early braking.

Most current AEB systems lack information about road conditions and instead assume dry road conditions with a friction coefficient of 1. This assumption means that when braking autonomously on a low-friction surface, the intervention may be initiated too late. To initiate braking earlier but avoid unnecessary interventions, [43] used a warning brake to get the current friction estimate and reassess the amount of braking needed. This approach is clever if friction does not vary ahead. With predictive friction information, the braking distance for a varying friction profile can be calculated using a method as in [44]. However, predictive friction estimates are often inaccurate.

A missing key piece of the puzzle is the effect of incorrect friction estima-

tion on the braking distance. The next section presents the mathematical background for explaining misestimation in AEB systems, while the results are presented in Section 4.1.

Friction estimate properties

Friction estimation deviations can be transformed into braking distance deviations using (3.5). The *road friction deviation* is defined as the difference between the estimated friction μ_e and the real friction μ_r

$$e_\mu = \mu_e - \mu_r. \tag{3.7}$$

Similarly, the *braking distance deviation* is defined using (3.5) as

$$\begin{aligned} e_s =& s_e - s_r, \\ =& \frac{V_0^2}{2\,g}\left(\frac{1}{\mu_e} - \frac{1}{\mu_r}\right), \end{aligned} \tag{3.8}$$

where s_e is the estimated braking distance and s_r is the real braking distance.

The consequence of friction overestimation, i.e., $e_\mu > 0$, can be better understood by reformulating the residual distance into an impact velocity for a forward collision (*Paper A*). The *impact velocity* V_p is calculated from (3.5) setting the distance up to collision s equal to the estimated s_e as

$$\begin{aligned} s =& \frac{V_0^2 - V_p^2}{2\,g\,\mu_r} \xrightarrow{s=s_e}, \\ \frac{V_0^2}{2\,g\,\mu_e} =& \frac{V_0^2 - V_p^2}{2\,g\,\mu_r} \xrightarrow{\mu_e>\mu_r}, \\ V_p =& V_0\sqrt{\frac{e_\mu}{\mu_e}}. \end{aligned} \tag{3.9}$$

Impact velocity is useful for categorizing crash severity according to ASIL classification. An analysis of this for an AEB system was conducted in [29], suggesting the categorization presented in Table 3.1, which illustrates the severity of front and rear collisions as a function of impact velocity. These values can also be used to assess the consequences of friction misestimation in AEB systems, which falls under SOTIF considerations rather than ASIL, as it stems from limitations in environmental perception rather than system failure.

Table 3.1: Severity index ASIL classification for a Front-/Rear-end collision [29]

Class	S_0	S_1	S_2	S_3
Description	no injuries	light & moderate injuries	severe injuries	life-threatening injuries
Front/Rear-end collision	no harms to persons	$v_p < 20$ km/h	$20 < v_p < 40$ km/h	$v_p > 40$ km/h

Now that the impact velocity is mapped to the severity index, it can be related back to the distance deviation by replacing (3.9) into (3.8) as

$$e_s = -\frac{V_p^2}{2\,g\,\mu_r}. \tag{3.10}$$

The analysis of the impact of friction estimation deviations on braking distance and impact velocity is presented in Section 4.1. In addition to estimation deviations, friction itself can vary naturally along the road, affecting the applicability of the average friction coefficient $\bar{\mu}$ defined in (3.6). Section 4.2 presents a methodology to explore and quantify these natural variations for locally uniform roads.

3.3 Braking with Steering: Handling Non-Uniform Road Conditions

So far, we have handled cases with minimal steering involvement. Introducing steering changes the vehicle's dynamic behavior, rendering the previously used equations largely invalid. This is typically the case on non-uniform, non-straight roads.

Braking on split friction roads

Papers B, C addressed the special case of braking on a split friction road, where one half of the vehicle is on high friction and the other half on low friction, as illustrated in Fig. 3.3. The key challenge in this scenario is the abrupt yaw moment disturbance (M_z) caused by asymmetric road friction. Unprepared drivers may be surprised and either deviate from their path during

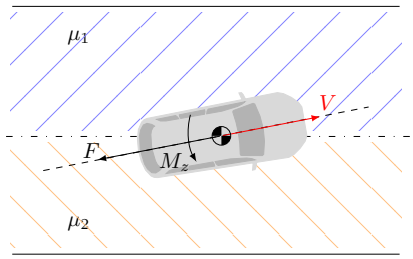

Figure 3.3: Vehicle on a split friction road.

braking [45] or release the brakes. Steering must be applied to counteract the yaw disturbance and keep the vehicle in its lane, but this is not an easy task.

Much of the literature assumes that ABS alone can effectively maintain stability while braking in these conditions [46]–[48]. However, this assumption breaks down at large split friction magnitudes. As analyzed in *Paper B*, traditional ABS algorithms limit slip on the rear axle [49], preventing an increase beyond the peak slip on the low-friction side—an adjustment necessary for large splits. Additionally, ESC systems often restrict yaw torque by reducing braking on the high-friction side [50], leading to longer braking distances. These findings indicate that a redesign of ABS and ESC strategies is necessary for effective handling of high split friction conditions.

Previous literature has primarily focused on automating steering compensation while allowing the ABS to manage braking [46]–[48]. Others proposed ABS modifications for split friction [51], but without controlling steering. More recent studies [52], [53] have combined braking and steering control. In [52], ABS was redesigned to account for combined slip and coupled with a steering controller. Their fuzzy control allocation scheme first determines the steering angle to maintain stability and a straight path, then computes brake forces to achieve zero yaw torque. This method was later extended to curved roads in [54]. However, a key limitation of this approach is its reliance on tyre model inversion, which is impractical due to real-world tyre variations from wear, pressure, and temperature changes [13], [37], as well as between manufacturers and tyre types. Furthermore, their strategy restricted slip to remain below the peak, which, as we show, is suboptimal for large split friction magnitudes.

In [53], an integrated steering and braking MPC controller was proposed for a bus and verified on a test bench. The study used yaw acceleration as a threshold for identifying large split friction cases and selecting a control strategy accordingly. *Paper B* similarly differentiates between small and large split friction cases, but instead of relying on an arbitrary yaw acceleration threshold, it bases the transition on static optimal solution characteristics that vary with split friction magnitude. This allows a split friction estimate to determine the threshold for switching control strategies. Moreover, [53] limited wheel slips to the linear region only for high-friction tyres, which is less restrictive than doing so for the low-friction tyres. Still, they did not evaluate their control strategy at large splits or analyze its limitations, as done in *Paper B*.

The key results and insights from the analysis of split friction roads are presented in Section 4.3, while the next section introduces the optimization method.

Static optimization

The core idea of *Paper B* is that the high-level optimization problem (3.1) can be reduced to a static problem once transients have settled. This analysis has been conducted for straight, even roads. Instead, *Paper C* expanded the static optimization to curved roads.

For straight split friction roads, a quasi-steady-state solution exists, where deceleration remains constant and velocity eventually reaches zero. Since this static solution yields maximum braking, reaching it as quickly as possible leads to the shortest braking distance. The advantage of a static solution lies in its computational efficiency and its ability to provide insights into brake force and steering combinations that achieve maximum braking.

For a straight road, the optimization problem from (3.2) becomes static by setting the derivatives to zero, yielding the maximum static deceleration problem formulation

$$\begin{aligned} \min_{q} \quad & a_v(q), \\ \text{s.t.} \quad & a_p(q) = 0, \\ & M_z(q) = 0, \\ & \dot{\psi} = 0, \end{aligned} \tag{3.11}$$

where q represents the optimization variables

$$q = \left[\kappa_i, \delta, \beta\right]^\mathsf{T}, \tag{3.12}$$

which include the brake controls, represented by the longitudinal slips κ_i, and the steering-related variables δ and β. The optimization also considers the friction coefficients on each vehicle side, $[\mu_1, \mu_2]$. The accelerations a_v and a_p are given by (2.15), and the yaw moment M_z by (2.23).

The zero yaw rate condition, $\dot{\psi} = 0$, is imposed to prevent vehicle rotation. This constraint expresses the lateral slip angles as a function of β and δ

$$\tan \alpha_i = \left[\delta - \beta, \delta - \beta, -\beta, -\beta\right]^\mathsf{T}. \tag{3.13}$$

Next, we discuss roads with lateral friction variations, where careful path planning is essential to minimize braking distance.

Optimal braking path on varying friction roads

In the previous sections, path planning during braking was unnecessary, as the vehicle always brakes along the centerline, whether the road is straight or curved. This is because there are either no lateral friction variations or, in the case of split friction, lateral movement is undesirable. However, in *Paper D*, we demonstrated that when friction varies laterally, the shortest braking distance may not be achieved by staying on the centerline. In such cases, lateral vehicle movement becomes crucial for minimizing braking distance. Figure 3.4 illustrates an example where avoiding an icy patch could potentially lead to a shorter stopping distance. Knowing the friction distribution in advance can provide significant benefits in such scenarios.

Paper D investigated full-trajectory optimization to determine the optimal path, i.e., the trajectory that results in the shortest braking distance, by allowing lateral movement while braking. The objective is to minimize the final centerline position s_f of the vehicle while ensuring that it remains within the lane limits $[e_{\min}, e_{\max}]$ (see Fig. 2.1). This optimal control problem (OCP)

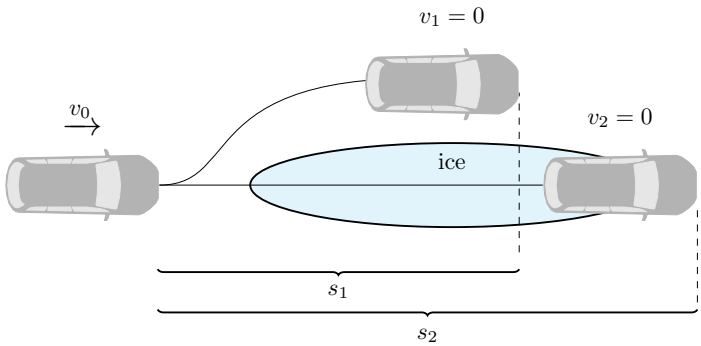

Figure 3.4: Two braking distance candidates: Moving laterally can result in faster stopping (*Paper D*).

is formulated as

$$\begin{aligned} \underset{\boldsymbol{x},\boldsymbol{u}}{\text{minimize}} \quad & s_f \\ \text{subject to} \quad & \dot{\boldsymbol{x}}(s) = G(\boldsymbol{x}(s), \boldsymbol{u}(s)), \\ & \{\boldsymbol{x}(0) = x_0,\ V_f \leq V_{stop}\}, \\ & e_{\min} \leq e(s) \leq e_{\max}, \\ & g(\boldsymbol{x}(s), \boldsymbol{u}(s)) = 0, \\ & h(\boldsymbol{x}(s), \boldsymbol{u}(s)) \leq 0 \end{aligned} \tag{3.14}$$

where $\boldsymbol{x}(s) \in \mathbb{R}^{n_x}$ and $\boldsymbol{u}(s) \in \mathbb{R}^{n_u}$ denote the vehicle state and control vectors, respectively. The function $G(\boldsymbol{x}(s), \boldsymbol{u}(s))$ represents the vehicle dynamics in space coordinates (PM: (2.10), ST & DT: (2.17)). Furthermore, the initial conditions are defined by x_0, while the final condition ensures that the velocity V_f is reduced to a sufficiently small value, determined by an appropriate threshold $V_{stop} > 0$. This threshold is necessary because the inverse path dynamics S_p (2.8) becomes singular as V approaches zero. Finally, $g(\cdot)$ and $h(\cdot)$ represent all other equality and inequality constraints, respectively. For instance, $h(\cdot)$ includes the friction limits (PM: (2.11), ST & DT: (2.29)), while $g(\cdot)$ includes equality constraints specific to the multiple-shooting optimization method used.

Applying the above OCP to different vehicle models requires an appropriate adaptation of the road friction profile when simplifying the vehicle model: for

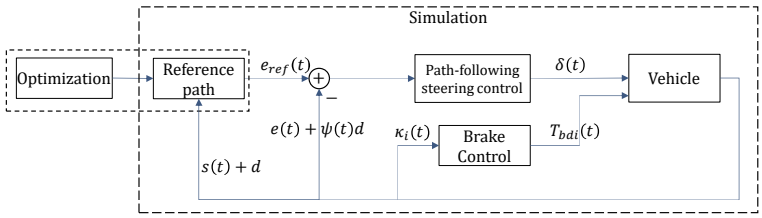

Figure 3.5: Closed-loop simulation block diagram in CarMaker$^{\text{TM}}$, where $s(t)$ is the longitudinal distance as a function of time t, $e(t)$ the lateral distance, d a chosen preview distance, $\dot{\psi}(t)$ the yaw rate, $\delta(t)$ the front steering angle, $\kappa_i(t)$ the long. slip, and $T_{bdi}(t)$ the brake torque demand for each tyre i (adapted from *Paper D*).

the ST model, the friction is averaged per axle from the four tyres of the DT model, while for the PM, a single equivalent friction value represents the entire vehicle since it lacks individual tyres.

The optimization problems discussed here form the basis for determining optimal vehicle trajectories and the distribution of braking and steering forces. To translate these theoretical results into practical vehicle control, a dedicated control framework is required, which is introduced in the next section.

Control structure overview

In *Papers B, C, D*, a similar control structure is implemented within the simulation environment CarMaker$^{\text{TM}}$. The block diagram is presented in Fig. 3.5.

In *Papers B & C*, the steering controller consists of a constant feedforward component, determined based on the split friction magnitude, and a path-following controller that previews the path ahead at a selected preview distance, following [16, Chapter 13]. The brake controller for split friction conditions regulates the high-friction brakes to eliminate yaw torque using Lyapunov theory [55] for large split friction magnitudes, while ABS is employed for small splits and always on the low-friction side. The details of this control strategy are explained in Section 4.3.

In contrast, *Paper D* adopts a much simpler control approach: the steering is managed solely by the path-following controller, and braking is handled entirely by the ABS.

CHAPTER 4

Road friction influence on braking distance

4.1 Braking Distance Estimate Deviations

Braking distance estimates used in AEB systems are inaccurate when the average friction coefficient of the braking path deviates from the assumed value. This section evaluates the impact of friction misestimation on the braking distance.

Following the methods of Section 3.2, Fig. 4.1 presents the braking distance deviations e_s as a function of the friction estimate deviation e_μ at a high, medium, and low friction. Setting an e_μ deviation to a small value of 0.1, it becomes clear that the lower the friction, the higher the braking distance deviation. In other words, the lower the friction, the more accuracy is needed in the estimates.

The braking distance deviations of the figure are also influenced by the square of the initial speed (3.8). Therefore, the higher the initial speed, the larger the expected deviations on the braking distance.

Overestimating friction might result in a collision. The impact speed thresholds for the ASIL classes are noted in Fig. 4.1 for the medium ($\mu_r = 0.5$) and low friction ($\mu_r = 0.25$) using (3.10). At high real friction, there is no misesti-

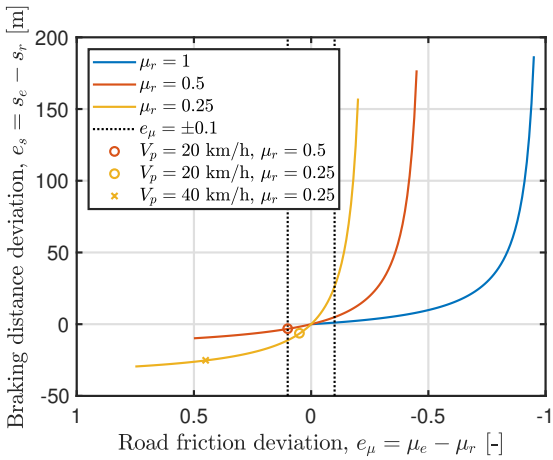

Figure 4.1: Effect of road friction estimation deviation on braking distance for a initial speed of 50 km/h; true friction μ_r, estimated friction μ_e, V_p impact speed. Positive braking distance deviations indicate braking earlier than expected, while negative deviations suggest braking later than expected, potentially leading to a collision.

mation. The severity indexes can then be updated according to Table 3.1, and the results are presented in Table 4.1. The friction deviation thresholds for transitioning from S_1 to S_2 are quite small: 0.1 for medium friction and 0.05 for low friction. Consequently, an AEB system that assumes dry friction can significantly increase the risk of severe injuries at medium friction and even cause life-threatening consequences (S_3) at low friction. System safety engineers can use a table like this to assess the margin for deviation at different speeds and road friction levels.

4.2 Natural Friction Variation of a Locally Uniform Road

Using measurements from the same area and under uniform conditions, one can reveal the combined *natural variation* of the road conditions and the vehicle's braking ability. This was the core idea behind *Paper A*, where measurements from a vehicle braking were evaluated under several uniform snowy/icy

Table 4.1: Severity index example for a Front-/Rear-end collision according to the specification of Table 3.1, in the same setting as Fig. 4.1

Real friction	Friction deviation threshold		Severity index
high	N/A		S_0
medium	0.1	$<$	S_1
		$>$	S_2
low	0.05	$<$	S_1
		between	S_2
	0.45	$>$	S_3

conditions. Next, the methodology used in the paper is briefly described, which involves using full-vehicle ABS braking measurements.

Friction and distance uncertainties from measurements

Solving (3.5) for μ and applying it to the speed and distance measurements, a set of estimates $\hat{\boldsymbol{\mu}} = \left[\hat{\mu}_1, \ldots, \hat{\mu}_N\right]^\intercal$ is obtained. Taking the maximum minus the minimum of the set, the friction uncertainty is given by

$$\hat{\delta}_\mu = \max(\hat{\boldsymbol{\mu}}) - \min(\hat{\boldsymbol{\mu}}). \tag{4.1}$$

An estimate of the braking distance can be obtained from (3.5). By taking the difference between the maximum and minimum braking distances, the uncertainty in braking distance can be calculated as follows

$$\begin{aligned} \hat{\delta}_s &= \max(s) - \min(s), \\ &= \frac{v_0^2}{2g}\left(\frac{1}{\min(\hat{\boldsymbol{\mu}})} - \frac{1}{\max(\hat{\boldsymbol{\mu}})}\right). \end{aligned} \tag{4.2}$$

A necessary step for this calculation is to ensure the same initial velocity is used for the entire dataset during the data post-processing. Next, the results are presented in brief.

Brake event data synopsis

Three different tyre types were fitted to the same vehicle, and a variety of snowy and icy conditions were prepared on a test track in northern Sweden

over a five-day period. The road was prepared to have a uniform friction profile. The results are presented in *Paper A*, and the key findings are discussed here. For related research with the same data, see [56].

The uncertainty in friction measures, $\hat{\delta}_\mu$ from (4.1), was generally small, ranging from 0.04 to 0.08, which can be considered the lowest variation expected due to the test preparation conditions. However, even such small variations in friction estimates can result in large braking distance deviations, as shown in Fig. 4.1. Additionally, negligible dependencies of friction were observed at the low and medium speeds tested.

Local variability of friction was revealed when projecting the brake events onto a map, as shown in Fig. 4.2. This variability was observed for the snow conditions (*snow, packed snow*) across all tyres, but not for the ice conditions (*smooth ice, rough ice, rougher ice*). This difference could be due to the lower mean friction of ice ($\bar{\boldsymbol{\mu}} = [0.07, 0.11, 0.18]$) compared to snow ($\bar{\boldsymbol{\mu}} = [0.35, 0.41]$). Two areas were identified, with a buffer zone in between where results were mixed. Therefore, local road properties are an important aspect of the experienced friction.

4.3 Understanding Split Friction: From Braking Limits to Control

Paper B provides an in-depth explanation of the combined braking and steering mechanics required to achieve maximum braking on split-friction roads. It also demonstrates, through simulations, the physical limits of combined braking and steering as a function of the split friction magnitude. These limits serve as a benchmark for evaluating control algorithms designed to optimize braking efficiency.

Paper C extends the analysis by investigating how optimal braking and steering characteristics change due to lateral load transfer in curved roads. A key insight is that when friction is lower on the inner curve side, the lateral load transfer further reduces the tyre capacity on that side, making the situation more critical than when friction is lower on the outer curve side.

These findings emphasize two crucial aspects: (1) the need to jointly optimize braking and steering to manage asymmetric road conditions effectively, and (2) the importance of adapting the solution based on the split friction magnitude. The next section provides a more detailed discussion on optimal

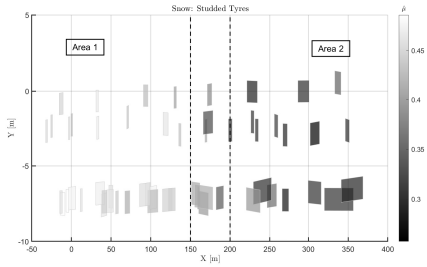

(a)

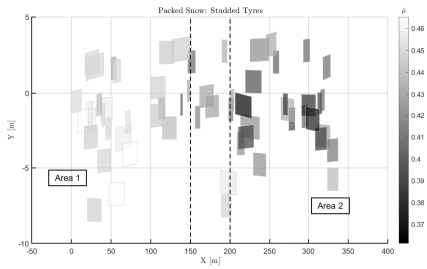

(b)

Figure 4.2: Friction map of test region under (a) snow and (b) packed snow conditions. Two areas are identified (adapted from *Paper A*).

brake force and steering angles, with control strategies addressed in the section thereafter.

Optimal brake force and steering angles

One of the key findings of *Paper B* is that, for small split-friction magnitudes, the peak slip and the optimal slip—i.e., the slip given by the static solution—coincide for the low-friction tyres. However, as the friction split increases, the optimal slip for the low-friction tyres shifts beyond the peak slip into the unstable slip region. This trend is illustrated in Fig. 4.3, which shows the peak and optimal slips for various low-friction side values (μ_2), while the high-friction side remains on dry asphalt (with $\mu_1 = 1$). For the high-friction tyres (not shown in the figure), the slip remains at the peak slip and stays close to it as the split increases.

A reason for this behavior was identified in the role of the steering. The lateral slip must reach a steady-state value determined only by the steering angle δ and body side slip angle β, as given by (3.13). Consequently, at the static solution (3.11), the body rotates slightly to achieve the angle β, allowing the rear axle to generate slip. To facilitate this body rotation, an initial front steering angle δ is required. The necessary steering and body slip are determined by the optimization.

The optimal solution can be visualized using attainable global force diagrams, as shown in [57], [58]. The methodology starts by discretizing the input vector $q = \left[\kappa_i, \delta, \beta\right]^\intercal$ from (3.12). The longitudinal slips κ_i were varied in the range $\kappa_i \in [0, -0.2]$, while the steering angle δ was sampled in the range $\delta \in [0°, -20°]$, and the body slip angles in the range $\beta \in [0°, -10°]$. Each of these ranges was discretized into $N = 10$ points, resulting in a total of N^6 input combinations.

Figure 4.4 illustrates the attainable force distribution in the three planes. The maximum deceleration (a_v) for zero yaw torque (M_z) and zero perpendicular acceleration (a_p) occurs at the optimal value $q^* = [\kappa_i^*, \delta^*, \beta^*] \approx -[0.11, 0.11, 0.08, 0.08, 4°, 2°]^\intercal$. The resolution difference between this brute-force method and the static optimization is within the second decimal place for κ_i and the first decimal place for the angles $[\delta, \beta]$ (in degrees). Furthermore, the optimal point (marked with a red cross in the figure) is located at the intersection of the $\{M_z = 0\}$-constraint, the $\{a_p = 0\}$-constraint, and the attainable force surface. Notably, in the a_v-M_z plane (Fig.4.4a), this point is located at the edge of the attainable force surface, aligning with the $\{M_z = 0\}$-constraint.

This observation connects to previous optimization-based research: [58] studied post-impact dynamics, while [59] analyzed lateral collision avoidance. Both studies found that the optimal solution maximizes lateral force (almost equal to a_p) while maintaining zero yaw moment (M_z) in steady-state conditions. In their findings, the optimal point also lies at the edge of the attainable force surface. In contrast, this study focuses on maximizing braking force. The observed alignment suggests a promising direction for extending the static optimization framework into trajectory optimization.

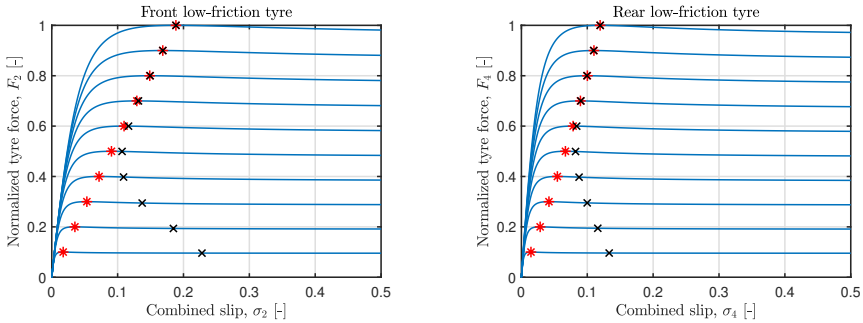

(a) **(b)**

Figure 4.3: Tyre force - slip curve for the low-friction tyres for several road frictions under split friction with $\mu_1 = 1$; $\mu_2 \in [0.1\ 1]$. The figure shows how the optimal slip moves away from peak slip as split friction increases. Marked with '*' are the peak slips and with 'x' the optimal slips. The high-friction tyres are at the vicinity of the peak slip.

Control aspects

Now that we know the static equilibrium the vehicle should be in to achieve maximum braking, we need to bring the vehicle to that state and maintain it throughout the braking maneuver. For small friction splits, this is a straightforward task, as the slips of all wheels are at peak slip. In this case, ABS provides optimal braking. However, for large friction splits, a more sophisticated approach is required, which involves balancing yaw torque from braking and counter-steering. The chosen approach is to fix the steering to an offline optimal value and control the high-friction brakes such that the yaw moment becomes zero.

A few considerations on the control:

1. **Inexact steering application:** The body slip angle β is largely influenced by the steering angle δ. Therefore, inaccurate steering application leads to an incorrect body slip angle and, consequently, a suboptimal equilibrium. Insufficient steering reduces braking effectiveness, whereas excessive steering causes braking saturation and can ultimately lead to vehicle instability (see Fig. 13 of *Paper B*).

2. **Path deviations:** Due to the combined effects of braking-induced yaw

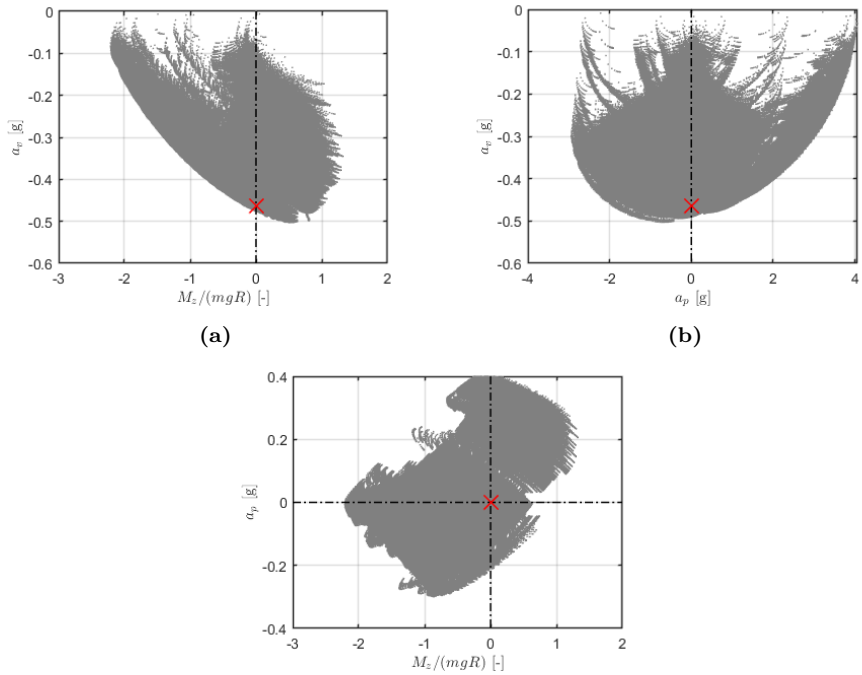

Figure 4.4: Attainable global force distribution for $\kappa_i \in [0, -0.2]$, $\delta \in [0°, -20°]$, $\beta \in [0°, -10°]$: (a) deceleration - yaw moment (a_v - M_z), (b) deceleration - perpendicular acceleration (a_v - a_p), (c) perpendicular acceleration - yaw moment (a_p - M_z). Red 'x' marks the optimal solution and dash-dotted curves denote the constraints. Optimal solution occurs for $[\kappa_i, \delta, \beta] \approx -[0.11, 0.11, 0.08, 0.08, 4°, 2°]^\intercal$. Large split with: $\mu_1 = 0.8$; $\mu_2 = 0.2$

moment and tyre saturation, full braking can lead to a loss of directional control and cause path deviations. Regaining control requires reducing the braking force, which can be achieved by applying a steering angle smaller than the optimal. However, this compromises braking performance and results in suboptimal deceleration.

3. **Steering application delays:** Since counter-steering is required to balance the yaw moment, any delays in steering application will delay brake force buildup and result in longer braking distances. The delay caused by a prepared professional human driver was measured and reproduced in simulation. These human-induced delays resulted in a 6%-13% increase in braking distances, which represents the best performance achievable by a human. Additionally, a few samples of close-to-limit braking are required to estimate the friction on each side of the vehicle and construct a split friction estimate for the algorithm to begin applying counter-steering. This process is fast enough, but a small benefit can be gained by having pre-information about the road's friction profile.

4.4 Lateral Movement for Shorter Braking

Paper D investigates the optimality of the paths generated using the OCP (3.14) in three road friction profiles: *(i)* partial snow cover, *(ii)* snow-tracks, and *(iii)* water puddles. The paths generated using the PM closely match those from the ST model. The PM-generated paths are then perturbed in simulation to verify their optimality. Although the PM does not provide the overall optimal path, it comes close; see the results in Table 4.2. This is attributed to the tyre model used in the simulation, which includes transient effects that enable the tyre to exert more force than in steady state.

In the examined cases, the optimal paths tend to move towards areas of higher friction, aligning with human driver intuition. However, since drivers typically avoid steering in critical situations, incorporating autonomous steering into an AEB system should be considered.

Table 4.2: Braking distances from optimization and simulation for friction profile (i), comparing the particle model (PM), single-track (ST), and the overall optimal solution; $V_0 = 30$ m/s (adapted from *Paper D*).

		Braking distance	
		absolute [m]	relative to shortest [%]
OCP	PM	83.9	1.8
	ST	84.2	2.2
simulation	w/ PM path	84.0	1.9
	w/ ST path	84.0	1.9
	total optimal	82.4	ref
	no steering	102.3	24.2

CHAPTER 5

Summary of included papers

This chapter provides a summary of the included papers.

5.1 Paper A

Ektor Karyotakis, Derong Yang, Mats Jonasson, Jonas Sjöberg
Experimental Study on Road Friction Variation and Stopping Distance Uncertainty using ABS Braking Data
Presented in *AVEC'22*,

This paper investigates the remaining fluctuation of road friction and stopping distance when the contribution from known sources has been removed. This fluctuation can serve as uncertainty for active safety functions relying

on friction estimates. Data from repeated ABS brake maneuvers on several uniform road conditions, including high and low friction surfaces, is analyzed. Road friction estimates are obtained and used to estimate the uncertainty in road friction and stopping distance. Measurements from the same road segment show a friction uncertainty of less than 0.1 with the presented procedure. The stopping distance uncertainty becomes considerable at high speeds and low friction for the intended use in emergency brake functions. Especially for low friction, high estimate accuracy is motivated.

EK contributed with ideas, implementation, generation and analysis of results. MJ, DY, and JS contributed to the idea generation and analysis of results. JS also contributed to the writing.

5.2 Paper B

Ektor Karyotakis, Mats Jonasson, Derong Yang, Jonas Sjöberg
Minimum Stopping Distance on Split Friction Roads via Joint Control of Steering and Individual Wheel Braking
Submitted to *Vehicle System Dynamics*,
in Sept. 2024.

This paper addresses the problem of minimizing stopping distance on split-friction roads through joint control of individual wheel brakes and automated steering. A static optimization problem is formulated to maximize braking while maintaining lane adherence. The analysis reveals two solution regions: for small split asymmetries, ABS and path-following control are sufficient; for large asymmetries, allowing higher slips at low-friction tyres enhances braking. A control framework leveraging feedforward steering and high-friction brake control is proposed and validated in CarMaker simulations. Compared to professional driver tests, automated steering reduces stopping distances by 6–13% and ensures effective braking even on zero-friction surfaces.

EK contributed with ideas, implementation, generation and analysis of results. MJ, DY, and JS contributed to the idea generation and analysis of results. JS also contributed to the writing.

5.3 Paper C

Ektor Karyotakis, Derong Yang, Mats Jonasson, Jonas Sjöberg
Optimal Braking and Steering Control Under Split Friction on Curved Roads
Published in *Lecture Notes in Mechanical Engineering*,
21954356 (ISSN) 21954364 (eISSN),
pp. 604–610, Conference: AVEC 2024.

This paper examines maximum deceleration on split friction curved roads. The optimal brake force and steering allocation is investigated as a function of the split friction asymmetry. Results show that low friction is more detrimental to maximum braking on the inner side of the curve due to load transfer. Finally, the paper showcases that the established control strategy of *Paper B* enhances safety and maneuverability in critical split friction curved roads.

EK contributed with ideas, implementation, generation and analysis of results. DY, MJ, and JS contributed to the idea generation.

5.4 Paper D

Ektor Karyotakis, Mats Jonasson, Derong Yang
Trajectory Optimization for Safe Stops with Laterally Varying Road Friction Ahead
Submitted to *IEEE Transactions of Intelligent Transportation Systems*, in March 2025.

This paper presents an optimal control approach for minimizing stopping distance by incorporating lateral variations in road friction. The paths leading to the shortest stopping distance are analyzed for three road friction profiles that vary across the road in the high-fidelity simulation environment

of CarMaker. A computationally efficient particle model is compared to a single-track vehicle model, demonstrating that the simpler model provides sufficiently accurate reference paths for road friction-based path planning. The paths generated from the particle model are perturbed in simulation and show near-optimal performance, closely matching those from the single-track model. The results highlight the importance of considering local friction variations, which are often neglected in advanced driver assistance systems.

EK contributed with ideas, implementation, generation and analysis of results. MJ and DY contributed to the idea generation and analysis of results.

CHAPTER 6

Concluding remarks and Future work

6.1 Concluding remarks

This thesis has investigated the combined braking and steering strategies that minimize the braking distance on roads with non-uniform friction. Two key aspects have been examined using optimization techniques and high-fidelity simulations: braking under split friction conditions and path optimization in the presence of lateral friction variations.

For braking on split friction roads, a static optimization was introduced to determine the optimal distribution of brake forces and steering inputs. The results demonstrate that traditional ABS-based braking is effective when the split friction magnitude is small. However, at larger splits, increased slips are required at the low-friction tyres, which cannot be achieved with traditional ABS. The proposed control framework was shown to achieve reductions in braking distance of up to 13% compared to a professional human driver.

Furthermore, this study explored the impact of lateral friction variations on braking performance. A trajectory optimization approach was developed to identify the paths that minimize braking distances when friction varies across the road's width. The findings reveal that even a simplified particle model

can generate near-optimal reference paths, closely matching those from a more complex vehicle model. This paves the way for friction-aware path planning.

The findings of this work highlight the potential benefits of predictive friction estimation for improving braking performance in future advanced driver assistance systems. They also stress the importance of coordinating braking and steering control in cases of extreme friction differences between the tyres.

6.2 Future work

The primary objective of this work is to develop an implementable friction-aware path and motion planning framework. This requires first analyzing the effects of road friction variations on path planning and braking distance predictions. Second, these methods should be extended to real-time implementation and experimentally validated under real-world driving conditions. Any control framework must account for friction estimation uncertainty, translating it into an acceptable risk based on the intended maneuver.

The first step for industrializing the friction-aware framework is to amend several ADAS functions by incorporating friction information with uncertainty. Both this and previous research indicate a substantial safety boost for current ADAS with friction information.

Future work could explore the fusion of local and predictive friction estimation to enhance adaptability to varying environmental conditions. These fused estimates can then be integrated into a unified control strategy to further improve the robustness and safety of motion and path planning decisions.

References

[1] Volvo Car Corporation, *Volvo cars puts 1000 test cars to use: Scandinavian cloud-based project for sharing road-condition information becomes a reality*, https://www.media.volvocars.com/global/en-gb/media/pressreleases/157065/volvo-cars-puts-1000-test-cars-to-use-scandinavian-cloud-based-project-for-sharing-road-condition-in, (accessed: 2025-02-21), 2015.

[2] S. Saha, P. Schramm, A. Nolan, and J. Hess, "Adverse weather conditions and fatal motor vehicle crashes in the united states, 1994-2012," *Environmental health*, vol. 15, pp. 1–9, 2016.

[3] F. Malin, I. Norros, and S. Innamaa, "Accident risk of road and weather conditions on different road types," *Accident Analysis & Prevention*, vol. 122, pp. 181–188, Jan. 2019, ISSN: 0001-4575.

[4] Y. Yin, H. Wen, L. Sun, and W. Hou, "The influence of road geometry on vehicle rollover and skidding," *International Journal of Environmental Research and Public Health*, vol. 17, no. 5, p. 1648, 2020.

[5] N. H. T. S. Administration, *Crash data by road surface conditions*, https://cdan.nhtsa.gov/query, Fatality and Injury Reporting System Tool (FIRST), 2025.

[6] D. P. Martin and G. F. Schaefer, "Tire-road friction in winter conditions for accident reconstruction," *SAE transactions*, pp. 732–750, 1996.

[7] K. N. de Winkel and M. Christoph, "Rethinking advanced driver assistance system taxonomies: A framework and inventory of real-world safety performance," *Transportation Research Interdisciplinary Perspectives*, vol. 29, p. 101 336, 2025, ISSN: 2590-1982.

[8] C. Lex, A. Eichberger, and I. Koglbauer, "Road condition estimation for automated driving considering drivers' acceptance," in *2nd IAVSD Workshop on Dynamics of Road Vehicles*, Technische Universität Berlin, 2017.

[9] T. Rahman, A. Liu, D. Cheema, V. Chirila, and D. Charlebois, "Adas reliability against weather conditions: Quantification of performance robustness," in *27th International Technical Conference on the Enhanced Safety of Vehicles (ESV) National Highway Traffic Safety Administration*, 2023.

[10] S. Zang, M. Ding, D. Smith, P. Tyler, T. Rakotoarivelo, and M. A. Kaafar, "The impact of adverse weather conditions on autonomous vehicles: How rain, snow, fog, and hail affect the performance of a self-driving car," *IEEE vehicular technology magazine*, vol. 14, no. 2, pp. 103–111, 2019.

[11] M. Acosta, S. Kanarachos, and M. Blundell, "Road friction virtual sensing: A review of estimation techniques with emphasis on low excitation approaches," *Applied Sciences*, vol. 7, p. 1230, 12 Nov. 2017, ISSN: 2076-3417.

[12] L. Chapman and J. E. Thornes, "Small-scale road surface temperature and condition variations across a road profile," in *Proceedings of the 14th SIRWEC Conference*, 2008.

[13] F. Gustafsson, "Slip-based tire-road friction estimation," *Automatica*, vol. 33, pp. 1087–1099, 6 Jun. 1997, ISSN: 00051098.

[14] S. Müller, M. Uchanski, and K. Hedrick, "Estimation of the maximum tire-road friction coefficient," *Journal of Dynamic Systems, Measurement, and Control*, vol. 125, pp. 607–617, 4 Dec. 2003, ISSN: 0022-0434.

[15] M. Choi, J. J. Oh, and S. B. Choi, "Linearized recursive least squares methods for real-time identification of tire–road friction coefficient," *IEEE Transactions on Vehicular Technology*, vol. 62, no. 7, pp. 2906–2918, 2013.

[16] R. Rajamani, *Vehicle Dynamics and Control*. Springer Science & Business Media, 2011.

[17] F. Crocetti, G. Costante, M. Fravolini, and P. Valigi, "A data-driven slip estimation approach for effective braking control under varying road conditions," in *2020 28th Mediterranean Conference on Control and Automation (MED)*, IEEE, Sep. 2020, pp. 496–501, ISBN: 978-1-7281-5742-9.

[18] A. Albinsson, F. Bruzelius, B. Jacobson, and J. Fredriksson, "Design of tyre force excitation for tyre–road friction estimation," *Vehicle System Dynamics*, vol. 55, pp. 208–230, 2 Feb. 2017, ISSN: 0042-3114.

[19] D. Yang and M. Jonasson, "Road friction estimation," US11543343B2, 2023.

[20] A. Niskanen, "Sensing the tyre-road contact by intelligent tyre," PhD Thesis, Aalto University, 2017, ISBN: 9789526075174.

[21] Y. Wu, F. Liu, L. Guan, and X. Yang, "A survey of vision-based road parameter estimating methods," in *Intelligent Computing Methodologies: 16th International Conference, ICIC 2020, Bari, Italy, October 2–5, 2020, Proceedings, Part III 16*, Springer, 2020, pp. 314–325.

[22] E. Šabanovič, V. Žuraulis, O. Prentkovskis, and V. Skrickij, "Identification of road-surface type using deep neural networks for friction coefficient estimation," *Sensors*, vol. 20, p. 612, 3 Jan. 2020, ISSN: 1424-8220.

[23] S. Roychowdhury, M. Zhao, A. Wallin, N. Ohlsson, and M. Jonasson, "Machine learning models for road surface and friction estimation using front-camera images," in *2018 International Joint Conference on Neural Networks (IJCNN)*, vol. 2018-July, IEEE, Jul. 2018, pp. 1–8, ISBN: 978-1-5090-6014-6.

[24] H. Karunasekera and J. Sjöberg, "In search for better road surface condition estimation - using non-road image region," *IEEE Intelligent Vehicles Symposium, Proceedings*, pp. 3205–3211, 2024, ISSN: 26427214.

[25] L. Svensson and M. Törngren, "Fusion of heterogeneous friction estimates for traction adaptive motion planning and control," in *2021 IEEE International Intelligent Transportation Systems Conference (ITSC)*, IEEE, 2021, pp. 424–431.

[26] J. Casselgren, M. Sjödahl, M. Sanfridsson, S. Woxneryd, J. Valldorf, and W. Gessner, "Classification of road conditions—to improve safety," in *Advanced Microsystems for Automotive Applications*, Springer, vol. 2, 2007, pp. 47–59.

[27] S. Sollén, "Monitoring winter road friction using floating car data," Licentiate Thesis, Luleå University of Technology, 2022.

[28] T. Weber, "On the potential of a weather-related road surface condition sensor using an adaptive generic framework in the context of future vehicle technology," PhD Thesis, Universität Duisburg-Essen, 2021.

[29] T. Ahrenhold, J. Iatropoulos, C. Pethe, and R. Henze, "Fat-schriftenreihe 355: Anforderungen an die güte, verfügbarkeit und vorausschau einer reibwertschätzung aus funktionssicht," Technische Universitat Braunschweig Institut fur Fahrzeugtechnik, Tech. Rep., 2022.

[30] T. Ahrenhold, J. Iatropoulos, and R. Henze, "Accuracy requirements for the road friction coefficient estimation of a friction-adaptive automatic emergency steer assist (esa)," *Automotive and Engine Technology*, vol. 8, no. 3, pp. 141–151, 2023.

[31] Y. Wang, J. Iatropoulos, S. Thal, and R. Henze, "Enhancing urban aeb systems: Simulation-based analysis of error tolerance in distance estimation and road-tire friction coefficients," SAE Technical Paper 2024-01-2992, Tech. Rep., 2024.

[32] G. Perantoni and D. J. Limebeer, "Optimal control for a formula one car with variable parameters," *Vehicle System Dynamics*, vol. 52, no. 5, pp. 653–678, 2014.

[33] V. Fors, P. Anistratov, B. Olofsson, and L. Nielsen, "Predictive force-centric emergency collision avoidance," *Journal of Dynamic Systems, Measurement, and Control*, vol. 143, no. 8, p. 081 005, 2021, ISSN: 0022-0434.

[34] M. Brown and J. C. Gerdes, "Robust stabilization and collision avoidance through minimizing open-loop velocity uncertainty," in *2020 IEEE Intelligent Vehicles Symposium (IV)*, IEEE, 2020, pp. 259–264.

[35] H. Pacejka, *Tire and Vehicle Dynamics*. Elsevier, 2005.

[36] V. Fors, L. Nielsen, and B. Olofsson, *Models for Optimization of Vehicle Maneuvers*. Vehicular Systems, ISY, Linköping University, 2023.

[37] J. Svendenius, "Tire modeling and friction estimation," PhD Thesis, Lund University, 2007.

[38] B. Jacobson, M. Jonasson, and F. Bruzelius, *Compendium in Vehicle Motion Engineering*. Chalmers University of Technology, 2023.

[39] T. D. Day and S. G. Roberts, "A simulation model for vehicle braking systems fitted with abs," *SAE Transactions, Section 6: Journal of Passenger Cars: MECHANICAL SYSTEMS*, vol. 111, pp. 821–839, 2002.

[40] D. Burton, A. Delaney, S. Newstead, D. Logan, and B. Fildes, "Evaluation of anti-lock braking systems effectiveness," Royal Automobile Club of Victoria (RACV), Tech. Rep., 2004.

[41] J. C. Hartman, H. Marzbani, F. Alam, M. Fard, and R. N. Jazar, "Friction coefficient of pneumatic tires and bitumen roads," *Nonlinear Approaches in Engineering Applications: Energy, Vibrations, and Modern Applications*, pp. 209–276, 2018.

[42] Volvo Car Corporation, *Safe space technology*, `https://www.volvocars.com/intl/safety/features/`, (accessed: 2025-04-04), 2025.

[43] Y. Hwang and S. B. Choi, "Adaptive collision avoidance using road friction information," *IEEE Transactions on Intelligent Transportation Systems*, vol. 20, no. 1, pp. 348–361, 2019.

[44] J. Herzfeld, S. Thottathodhi, M. Jonasson, L. S. Muppirisetty, S. Roychowdhury, and J. Sjöberg, "Collision avoidance by utilizing dynamic road friction information," in *2020 54th Asilomar Conference on Signals, Systems, and Computers*, IEEE, 2020, pp. 1425–1429.

[45] K. Tagesson, B. Jacobson, and L. Laine, "Driver response to automatic braking under split friction conditions," in *Proc. of the 12th International Symposium on Advanced Vehicle Control (AVEC)*, 2014, pp. 666–671.

[46] R. G. Hebden, C. Edwards, and S. K. Spurgeon, "Automotive steering control in a split-μ manoeuvre using an observer-based sliding mode controller," *Vehicle System Dynamics*, vol. 41, pp. 181–202, 3 Mar. 2004, ISSN: 00423114.

[47] L. Abi, D. Jin, S. Zheng, Z. Lu, and L. Yu, "Dynamic coordinated control strategy of autonomous vehicles during emergency braking under split friction conditions," *IET Intelligent Transport Systems*, vol. 15, pp. 1215–1227, 10 Oct. 2021, ISSN: 1751956X.

[48] L. Yu, S. Zheng, Y. Dai, L. Abi, X. Liu, and S. Cheng, "A feedback-feedforward steering controller designed for vehicle lane keeping in hard-braking manoeuvres on split-μ roads," *Vehicle System Dynamics*, vol. 60, pp. 1763–1787, 5 2022, ISSN: 17445159.

[49] R. V. V. Petrescu, "Mechatronic systems to the braking mechanisms," *Journal of Mechatronics and Robotics*, vol. 4.1, pp. 156–190, 2020.

[50] A. T. Van Zanten, "Bosch ESP systems: 5 years of experience," *SAE Transactions, Section 7: Journal of Passenger Cars: Electronic and Electrical systems*, vol. 109, pp. 428–436, 2000.

[51] E. Dong and L. Zhang, "Vehicle stability control system of emergency brake on split-mu road," *Proceedings - 9th International Conference on Intelligent Human-Machine Systems and Cybernetics, IHMSC 2017*, vol. 1, pp. 252–255, Sep. 2017.

[52] H. Mirzaeinejad, M. Mirzaei, and R. Kazemi, "Enhancement of vehicle braking performance on split-μ roads using optimal integrated control of steering and braking systems," *Proceedings of the Institution of Mechanical Engineers, Part K: Journal of Multi-body Dynamics*, vol. 230, pp. 401–415, 4 Dec. 2016, ISSN: 20413068.

[53] Z. Xue, C. Li, X. Wang, L. Li, and Z. Zhong, "Coordinated control of steer-by-wire and brake-by-wire for autonomous emergency braking on split-μ roads," *IET Intelligent Transport Systems*, vol. 14, pp. 2122–2132, 14 Dec. 2020, ISSN: 1751956X.

[54] M. Mirzaei and H. Mirzaeinejad, "Fuzzy scheduled optimal control of integrated vehicle braking and steering systems," *IEEE/ASME Transactions on Mechatronics*, vol. 22, pp. 2369–2379, 5 Oct. 2017, ISSN: 10834435.

[55] H. K. Khalil, *Nonlinear Control*. Pearson, 2015.

[56] M. Hjort, F. Bruzelius, S. Kharrazi, and D. Yang, "A method for obtaining reference friction values for validation of road friction estimation algorithms," in *16th International Symposium on Advanced Vehicle Control (AVEC 2024)*, G. Mastinu, F. Braghin, F. Cheli, M. Corno, and S. M. Savaresi, Eds., Springer Nature Switzerland, 2024, pp. 50–56, ISBN: 978-3-031-70392-8.

[57] M. Jonasson, J. Andreasson, B. Jacobson, and A. S. Trigell, "Global force potential of over-actuated vehicles," *Vehicle System Dynamics*, vol. 48, no. 9, pp. 983–998, 2010.

[58] D. Yang, T. J. Gordon, B. Jacobson, and M. Jonasson, "Quasi-linear optimal path controller applied to post impact vehicle dynamics," *IEEE Transactions on Intelligent Transportation Systems*, vol. 13, no. 4, pp. 1586–1598, 2012.

[59] V. Fors, B. Olofsson, and L. Nielsen, "Autonomous wary collision avoidance," *IEEE Transactions on Intelligent Vehicles*, vol. 6, no. 2, pp. 353–365, 2020.